Journal of Alloys and Compounds 509 (2011) 6049–6055

Contents lists available at ScienceDirect

Journal of Alloys and Compounds

journal homepage: www.elsevier.com/locate/jallcom

Phase transition and piezoelectric properties of $K_{0.48}Na_{0.52}NbO_3$–$LiTa_{0.5}Nb_{0.5}O_3$–$NaNbO_3$ lead-free ceramics

Gao Feng*, Liu Liangliang, Xu Bei, Cao Xiao, Deng Zhenqi, Tian Changsheng

School of Material Science and Engineering, Northwestern Polytechnical University, Xi'an, Shaanxi 710072, China

ARTICLE INFO

Article history:
Received 5 August 2010
Received in revised form 3 March 2011
Accepted 3 March 2011
Available online 10 March 2011

Keywords:
Lead-free ceramics
Phase transition
Dielectric relaxor
Piezoelectric property

ABSTRACT

Plate-like $NaNbO_3$ (NN) particles were used as the raw material to fabricate $(1-x)[0.93\,K_{0.48}Na_{0.52}NbO_3$–$0.07Li(Ta_{0.5}Nb_{0.5})O_3]$–$xNaNbO_3$ lead-free piezoelectric ceramics using a conventional ceramic process. The effects of NN on the crystal structure and piezoelectric properties of the ceramics were investigated. The results of X-ray diffraction suggest that the perovskite phase coexists with the $K_3Li_2Nb_5O_{15}$ phase, and the tilting of the oxygen octahedron is probably responsible for the evolution of the tungsten–bronze-typed $K_3Li_2Nb_5O_{15}$ phase. The Curie temperature (T_C) is shifted to lower temperature with increasing NN content. $(1-x)[0.93\,K_{0.48}Na_{0.52}NbO_3$–$0.07Li(Ta_{0.5}Nb_{0.5})O_3]$–$xNaNbO_3$ ceramics show obvious dielectric relaxor characteristics for $x > 0.03$, and the relaxor behavior of ceramics is strengthened by increasing NN content. Both the electromechanical coupling factor (k_p) and the piezoelectric constant (d_{33}) decrease with increasing amounts of NN. 0.01–0.03 mol of plate-like $NaNbO_3$ in $0.93\,K_{0.48}Na_{0.52}NbO_3$–$0.07Li(Ta_{0.5}Nb_{0.5})O_3$ gives the optimum content for preparing textured ceramics by the RTGG method.

1. Introduction

In recent years, the search for lead-free piezoelectric materials to replace $Pb(Ti,Zr)O_3$ (PZT) ceramics has become a very hot topic for the sake of environmental protection [1,2]. Among these materials, (K, Na) NbO_3 (KNN) ceramics are receiving considerable attention. Nevertheless, pure KNN ceramics are known to be difficult to process to full density by natural sintering, and the highest piezoelectric coefficient (d_{33}) was not more than 100 pC/N. In order to improve the densification and piezoelectric properties of KNN ceramics, the different additions were added into KNN to form new KNN-based ceramic systems, such as KNN–$LiSbO_3$ [3], KNN–$LiTaO_3$ [4,5], KNN–$LiSbO_3$–$LiTaO_3$ [6,7], KNN–$AgTaO_3$ [8], KNN–$BiScO_3$ [9], KNN–$BaTiO_3$ [10], and KNN–$(Bi_{0.5}Li_{0.5})TiO_3$ [11]. Although the piezoelectric coefficient (d_{33}) increases to 172–298 pC/N, it is still halfway to the most-desired high-end PZT property (with d_{33} = 500–600 pC/N).

Currently, it is reported that the method of controlling microstructure using grain orientation makes it possible to obtain ceramic materials with the desired properties by reactive-templated grain growth (RTGG) [12,13]. In this method, template particles must be large and shape anisotropic so that they can be oriented during tape casting and grown preferentially during the sintering stage [14,15]. Some shape anisotropic particles such as TiO_2, $SrTiO_3$, $Bi_4Ti_3O_{12}$, and $SrBi_4Ti_4O_{15}$ have been used as templates to fabricate textured lead free piezoelectric ceramics [16–18].

Our previous study [19] indicated that adding $Li(Ta_{0.5}Nb_{0.5})O_3$ (LTN) to $K_{0.48}Na_{0.52}NbO_3$ lead-free piezoelectric ceramics can effectively improve their piezoelectric properties. In addition, ceramics with the composition $0.93\,K_{0.48}Na_{0.52}NbO_3$–$0.07Li(Ta_{0.5}Nb_{0.5})O_3$ (0.93KNN–0.07LTN) have shown optimum piezoelectric properties. In this kind of lead-free material, $NaNbO_3$ (NN) is one of the most promising templates for seeding the phase formation. If plate-like $NaNbO_3$ particles can be used as the template, this will result in good extension grain growth relationship because of the similarity of the lattice structure between $NaNbO_3$ and the matrix material. However, before orienting by the RTGG method, the problem of what proportion of plate-like $NaNbO_3$ should be added to the 0.93KNN–0.07LTN ceramics must be solved, and the effect of the plate-like $NaNbO_3$ on the microstructure and piezoelectric properties needs to be understood.

In the present study, plate-like NN template particles were synthesized by the two-step NaCl–KCl molten salt process, and 0.93KNN–0.07LTN–*x*NN lead-free piezoelectric ceramics were

* Corresponding author. Tel.: +86 29 81038691.
E-mail address: gaofeng@nwpu.edu.cn (F. Gao).

0925-8388/$ – see front matter © 2011 Elsevier B.V. All rights reserved.
doi:10.1016/j.jallcom.2011.03.004

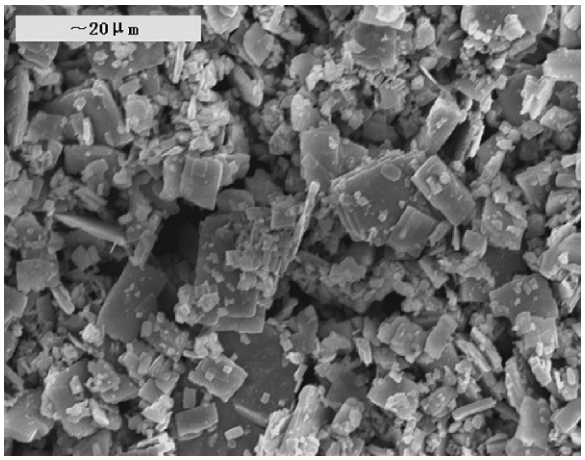

Fig. 1. SEM photograph of $NaNbO_3$ template particles.

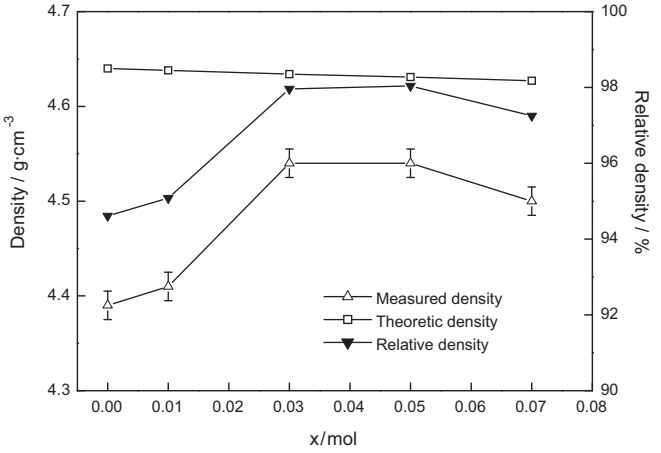

Fig. 2. Densities of 0.93KNN–0.07LTN–*x*NN ceramics.

fabricated. The effects of the plate-like $NaNbO_3$ on the phase structure and the electrical properties were investigated.

2. Experimental procedures

2.1. Preparation of plate-like $NaNbO_3$ templates

Plate-like $NaNbO_3$ (NN) template particles were prepared by the two-step NaCl–KCl molten salt synthesis (MSS) [20]. Reagent-grade Bi_2O_3, Na_2CO_3, Nb_2O_5, NaCl, and KCl were used as the starting materials. Firstly, bismuth layer-structured plate-like $Bi_{2.5}Na_{3.5}Nb_5O_{18}$ (BNN) particles with an average diameter of ~5 μm and a thickness of 1 μm were synthesized by the MSS method [21]. Secondly, using plate-like BNN as precursor, plate-like $NaNbO_3$ particles were synthesized using the chemical reaction shown in Eq. (1).

$$4Bi_{2.5}Na_{3.5}Nb_5O_{18} + 3Na_2CO_3 \rightarrow 20NaNbO_3 + 5Bi_2O_3 + 3CO_2\uparrow \quad (1)$$

The starting materials, plate-like $Bi_{2.5}Na_{3.5}Nb_5O_{18}$ and Na_2CO_3 (99%), were weighed to give a Na_2CO_3/BNN weight ratio of 1.50:1, then an equal weight of NaCl–KCl mixture was added to them. They were mixed by ball-milling in ethanol for 12 h and calcined in a sealed alumina crucible at 950 °C for 8 h. After slowly cooling to room temperature, the reaction product was washed ~10 times with hot de-ionized water and the NN template was separated using HNO_3 to remove the by-product Bi_2O_3. Then the powder was rewashed ~20 times with hot de-ionized water until no free Cl^- ions were detected using $AgNO_3$ solution. The NN templates were obtained by drying at 80 °C for 10 h. As shown in Fig. 1, the NN powder is formed of plate-like particles with an average diameter of 5–10 μm and a thickness of 1–2 μm; these can meet the needs of the RTGG method.

2.2. Fabrication of 0.93KNN–0.07LTN–xNN ceramics

The general formula of the material studied was $(1-x)[0.93\,K_{0.48}Na_{0.52}NbO_3$–$0.07Li(Ta_{0.5}Nb_{0.5})O_3]$–$xNaNbO_3$ (designated as 0.93KNN–0.07LTN–*x*NN), where *x* is 0.01, 0.03, 0.05, and 0.07. Reagent pure Na_2CO_3, K_2CO_3, Li_2CO_3, Nb_2O_5, and Ta_2O_5 were used as the starting materials. The mixtures were weighed stoichiometrically and ball-milled for 12 h. The powders were pre-calcined at 900 °C for 5 h. Then plate-like $NaNbO_3$ was added to the calcined powder and ball-milled for another 2 h. After milling and drying, the powder was pressed into disks 12.0 mm in diameter at 140 MPa, and then sintered at 1080 °C for 2 h. The sintered discs were polished and pasted with silver on both surfaces. Samples were poled at 120 °C for 20 min under an electric field of 4 kV/mm in silicone oil. The piezoelectric properties were measured after 24 h aging at room temperature.

2.3. Characterization

The crystal structures were determined by X-ray diffraction (XRD; model Panalytical X'Pert PRO, Holland) with 2θ in the range 15–60°. The microstructure was observed by scanning electron microscopy (SEM, Model Hitachi S-570, Japan). The average grain sizes were measured from 30 grains taken from at least three SEM micrographs from the same sample. The grain size distribution can be determined from SEM photos using an image processing and analysis program. The temperature dependence of the dielectric constant (ε) and the dielectric loss ($\tan\delta$) were measured between 30 °C and 500 °C with an LCR precision electric bridge (Model HP4284, Hewlett-Packard). The piezoelectric constant (d_{33}) was measured with a quasistatic piezoelectric d_{33}-meter (Model ZJ-3D, Institute of Acoustics Academic Sinica, China). The electromechanical coupling factor (k_p) and the electromechanical quality factor (Q_m) were determined by the resonance and anti-resonance technique using a precise impedance analyzer (Model HP4294A, Hewlett-Packard, CA).

3. Results and discussion

The densities of the 0.93KNN–0.07LTN–*x*NN ceramics were measured by the Archimedes method, and the theoretical density of the ceramics can be calculated by the XRD data using Riveteld method, which was similar to that of $(K_{0.48}Na_{0.52})(Nb_{0.95}Ta_{0.05})O_3$–$LiSbO_3$ ceramics [22]. Fig. 2 shows the change in the theoretical density, measured density, and relative density of the 0.93KNN–0.07LTN–*x*NN ceramics as a function of *x*. It was found that the theoretical density of the ceramics decreases slightly with increasing *x*. The results show that all the ceramics have relative densities higher than 94%, which means that the ceramics have achieved good densification under the experimental conditions used. The density increases from 4.41 to 4.54 g/cm^3. The maximum relative density, 98%, is achieved at $x = 0.03$–0.05. When the content of NN is higher than 0.05, the density decreases.

Previous studies [19] have indicated that the composition of 0.93KNN–0.07LTN ceramics lies in the morphotropic phase boundary, where the tetragonal ferroelectric phase coexists with the orthorhombic ferroelectric phase. Fig. 3 shows the XRD patterns of 0.93KNN–0.07LTN–*x*NN ceramics at room temperature. No

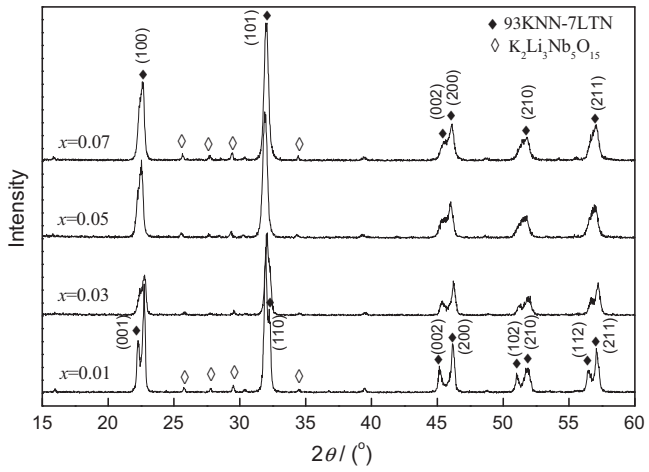

Fig. 3. X-ray diffraction patterns of the 0.93KNN–0.07LTN–*x*NN ceramics.

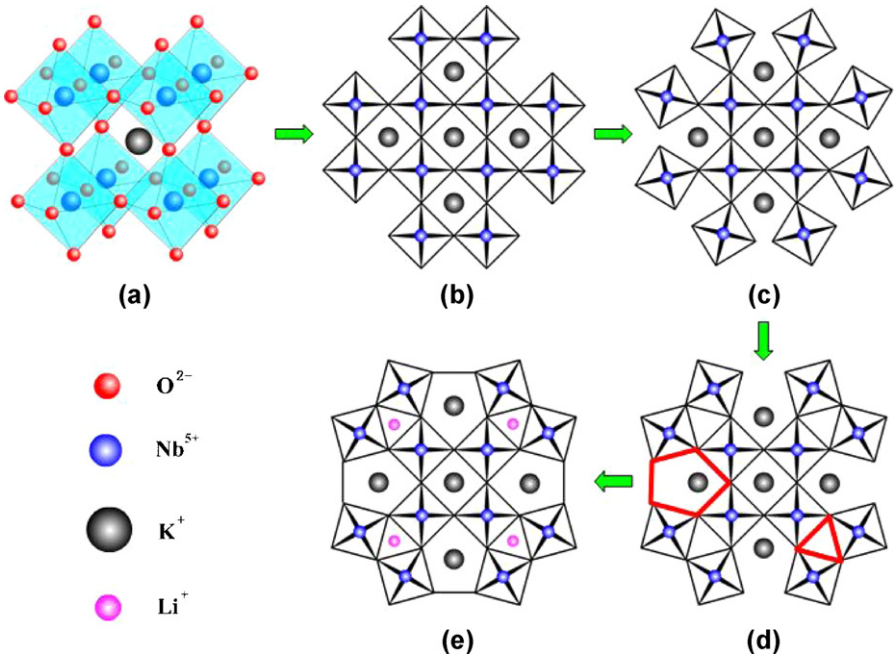

Fig. 4. A sketch showing the evolution of the $K_3Li_2Nb_5O_{15}$ crystal structure.

$NaNbO_3$ phase could be identified, which indicates that the NN has completely diffused into the 0.93KNN–0.07LTN lattice to form a new solid solution. It is found that the major phase of the system is the KNN–LTN solid solution with the perovskite structure, accompanied with a small quantity of a second phase $K_3Li_2Nb_5O_{15}$, with the tungsten bronze structure (TTB). Rubio-Marcos et al. also reported that the secondary phase with tungsten bronze structure is observed in KNN-based ceramics [23,24]. The relative content of $K_3Li_2Nb_5O_{15}$ was calculated using the intensity of the (1 1 0) peak for the perovskite and the (4 1 0) peak for the TTB phase [23]. The results show that the content of $K_3Li_2Nb_5O_{15}$ phase evolves toward a higher amount with increasing plate-like NN. Those were 3.68%, 4.03%, 4.70% and 4.74% for ceramics of $x = 0.01$, 0.03, 0.05, and 0.07, respectively.

When the proportion of $NaNbO_3$ is lower than 0.03 mol, it is observed that the double peaks of the perovskite phase appear, which demonstrates that the perovskite structure exhibits the major tetragonal symmetry. The structure transition can be determined from the double peaks at $2\theta \approx 22^\circ$, 32°, 52°, and 57°. The intensities of (0 0 1), (1 1 0), (1 0 2), and (1 1 2) decrease with increasing $NaNbO_3$. When the content of $NaNbO_3$ is greater than 0.05 mol, the (0 0 1), (1 1 0), (1 0 2), and (1 1 2) peaks disappear, and only the single (1 0 0), (1 0 1), (2 1 0), and (2 1 1) peaks remain. As x increases, the two diffraction peaks (0 0 2) and (2 0 0) start to merge into a broad single peak gradually, suggesting that the ceramic may have a tendency to transform from co-existing tetragonal and orthorhombic phases into pseudocubic phase at high addition levels of NN. Similar results have been reported for the CeO_2-doped KNN ceramics [25].

The ABO_3-type perovskite structure consists of the basic oxygen octahedron, as shown in Fig. 4(a) with Nb^{5+} (Ta^{5+}) occupying the center of the oxygen octahedra, while K^+ (Na^+) are located in the interstitial space between 8 oxygen octahedra. If we look at the structure from the ⟨0 0 1⟩ direction, the crystal structure can be described as an interstitial tetragonal space adjacent to oxygen octahedra, as shown in Fig. 4(b).

Before $NaNbO_3$ is added, the perovskite structure of 0.93KNN–0.07LTN ceramics is stable. It is well known that the stability of the ABO_3-typed perovskite structure can be evaluated by the tolerance factor t, which is given by the formula [26]:

$$t = \frac{r_A + r_O}{\sqrt{2}(r_B + r_O)} \quad (2)$$

where r_A and r_B are the ionic radii of the ions occupying the A, B positions, respectively, and r_O is the ionic radius of oxygen. It has been observed that a stable perovskite may be expected to form if $t = 0.77$–1.09. The closer the tolerance factor t approaches 1, the more stable the perovskite structure is. Table 1 shows the calculated tolerance factors. The tolerance factor t of $LiTa_{0.5}Nb_{0.5}O_3$ is only 0.7, which means $LiTa_{0.5}Nb_{0.5}O_3$ cannot form a stable perovskite structure, but a kind of pseudo-perovskite with $R3c$ symmetry. It reveals that the perovskite structure of $KNbO_3$ is much more stable than that of $NaNbO_3$. The greater the content of $NaNbO_3$, the less stable is the perovskite structure.

Because Na^+ has the same valence as K^+, the A-site ion, Na^+ may easily enter the A-site and replace K^+ without changing the electric charge. However, the substitution of Na^+ for K^+ induces lattice strain, which results in reducing the ability of the mixed system to crystallize with the perovskite structure. The connection between the adjacent oxygen octahedron deteriorates and the structure tends to rearrange to form another more stable state. Tilting of the oxygen octahedra has made it possible for some of the adjacent tetragonal spaces to be replaced by pentagonal and triangular interstitial spaces, as shown in Fig. 4(c) and (d). Pentagonal spaces have little influence on the K^+ located there originally, while the volume of the triangular space is too limited to contain any ions whose radius is larger than 79 pm. Lithium ion (Li^+), with radius of only 68 pm, can diffuse into the lattice and occupy the triangular

Table 1
Tolerance factor of the compound related to 0.93KNN–0.07LTN ceramics.

Compound	R_A (pm)	R_B (pm)	R_O (pm)	t
$KNbO_3$	133	70	140	0.92
$NaNbO_3$	95	70	140	0.79
$K_{0.48}Na_{0.52}NbO_3$	113	70	140	0.85
$LiTa_{0.5}Nb_{0.5}O_3$	68	70	140	0.70

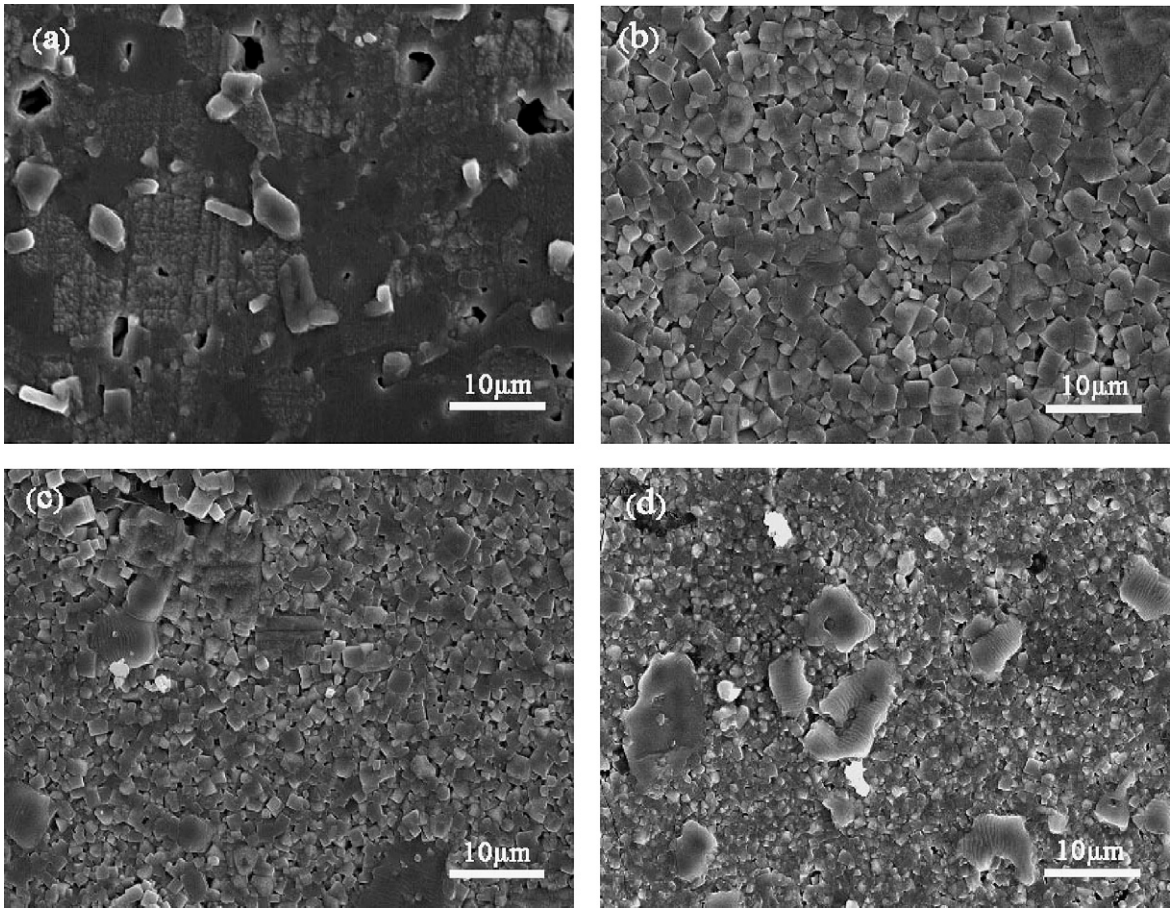

Fig. 5. SEM micrographs of 0.93KNN–0.07LTN–*x*NN ceramics. $x = 0.01$; (b) $x = 0.03$; (c) $x = 0.05$; (d) $x = 0.07$

space, which results in the formation of the tungsten–bronze-type $K_3Li_2Nb_5O_{15}$ compound, as shown in Fig. 4(e).

Fig. 5 shows the SEM micrographs of 0.93KNN–0.07LTN–*x*NN ceramics containing different amounts of NN. It is observed that the ceramics are sintered effectively with well-developed grains and are composed of two types of grain. One grain type is cubic with relatively small grain size; these are matrix grains. It is clear that the average grain size of the matrix grains decreases with increasing amounts of NN. An average grain size of ~10 μm is observed in 0.93KNN–0.07LTN–0.01NN ceramics, as seen in Fig. 5(a). Then the average grain size decreases to 2–3 μm. As well as the matrix grains, some irregularly shaped large grains were observed in the ceramics. There were no significant changes except the increasing proportion of large grains with increasing amounts of NN. It is concluded that these large grains are grown from the plate-like NN template grains. The density of the 0.93KNN–0.07LTN–0.01NN ceramics is relatively low (94.6%), while the ceramics of increasing *x* are generally larger than 97%. Therefore it was thought that adding a small amount of the plate-like NN can promote the densification of the KNN-based ceramics. Additionally, a few liquid phases are formed in the ceramics with high NN content, as shown in Fig. 5(d). The similar results were also observed in $CaTiO_3$-doped KNN-based ceramics [27].

Fig. 6 shows the room temperature dielectric response as a function of NN content. Whether measured at 1 kHz or 100 kHz, the dielectric constant ε decreases and then increases with increasing NN content, while the dielectric loss $\tan\delta$ continuously increases. The dielectric constant ε varies in the range of 750–950, and the dielectric loss $\tan\delta$ is less than 6%. Fig. 7 shows the dielectric properties of 0.93KNN–0.07LTN–*x*NN ceramics as a function of temperature using different measurement frequencies. For the 0.93KNN–0.07LTN–0.01NN sample, there are two dielectric peaks corresponding to an orthorhombic–tetragonal phase transition and the ferroelectric–paraelectric transition. Because orthorhombic–tetragonal phase transition occurs near to room temperature, this dielectric peak is not clearly seen from Fig. 7(a) and (b), while it can be observed obviously from Fig. 7(c) and (d). It shows that increasing the NN amount will shift the orthorhombic–tetragonal phase transition to far away from that of room temperature. Also, the addition of NN produces a slight broadening of the transition peak when the NN amount is >0.50.

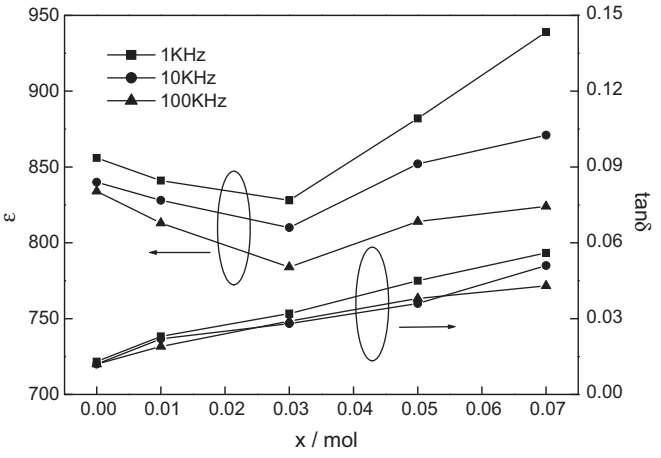

Fig. 6. The dielectric constant and loss of 0.93KNN–0.07LTN–*x*NN ceramics.

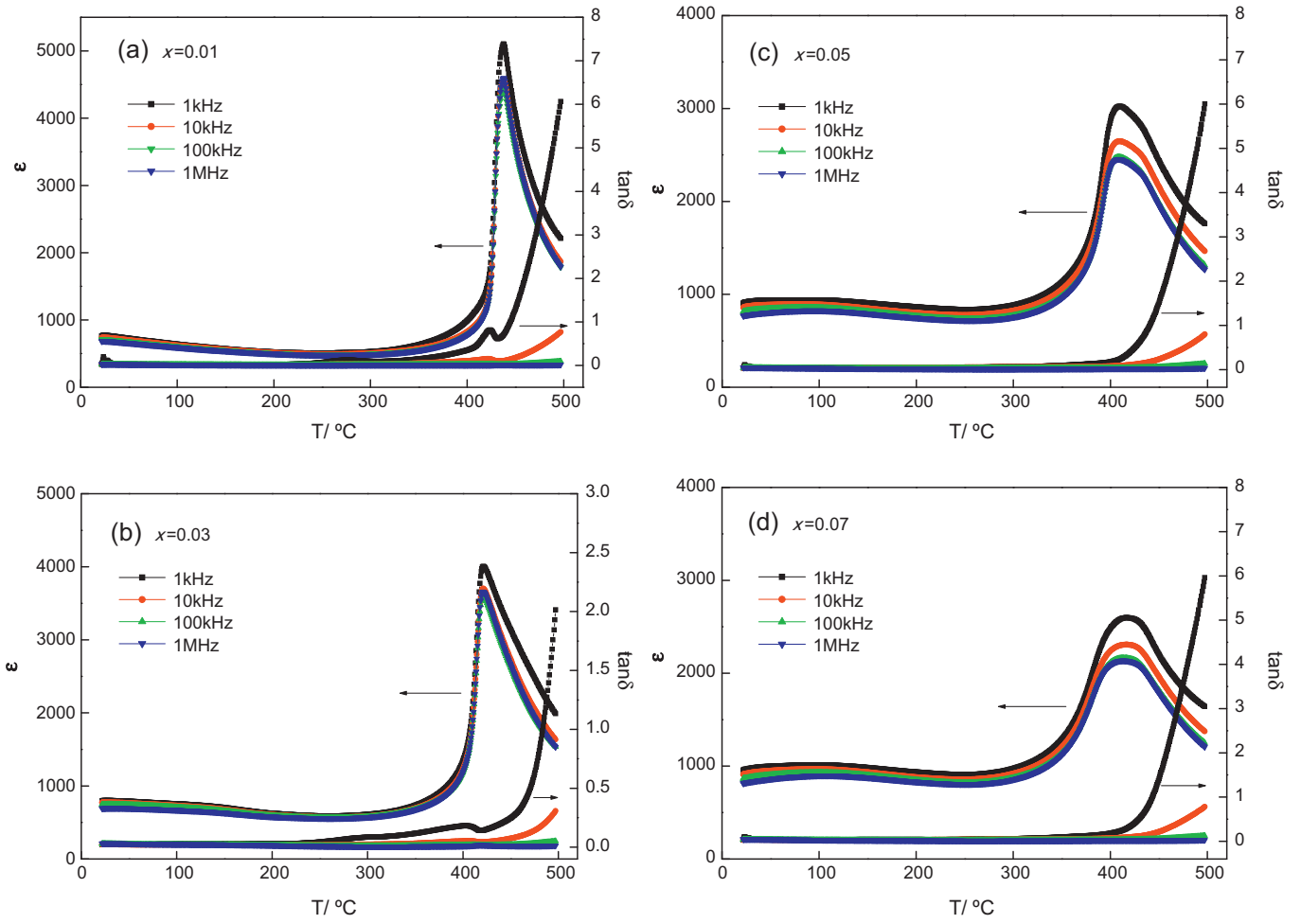

Fig. 7. The dielectric properties as a function of temperature for 0.93KNN–0.07LTN–*x*NN ceramics.

The dielectric constant continues to increase as the temperature rises above 400 °C, before exhibiting a relatively sharp dielectric peak near 440 °C. This transition corresponds to the ferroelectric–paraelectric phase transformation at the Curie temperature. For higher proportions of NN ($x > 0.03$), the dielectric peaks are significantly wider, suggesting diffuse phase transition characteristic, as shown in Fig. 7(c) and (d). What is more, the dielectric loss shows no obvious change until the temperature is higher than 400 °C. The value of $\tan\delta$ is found to become very large at high temperatures, indicating space charge polarization and associated ionic conductivity. As well as the diffuse phase transition, a strong frequency dispersion of the dielectric constant is clearly seen for the 0.93KNN–0.07LTN–*x*NN ceramics with $x > 0.03$. The maximum of the dielectric constant decreases as the measurement frequency increases.

The diffuseness of a phase transition can be determined from the modified Curie–Weiss law [28,29]:

$$\frac{1}{\varepsilon} - \frac{1}{\varepsilon_m} = C(T - T_m)^{\gamma} \quad (3)$$

where ε_m is the maximum value of dielectric constant at the phase transition temperature T_m, γ is the degree of diffuseness and C is the Curie-like constant. γ can range from 1, for a normal ferroelectric, to 2 for an ideal relaxor ferroelectric. Eq. (3) can be transformed into Eq. (4) by taking the logarithm of both sides.

$$ln\left(\frac{1}{\varepsilon} - \frac{1}{\varepsilon_m}\right) = \gamma \ln(T - T_m) + \ln C \quad (4)$$

From Eq. (4), $\ln(1/\varepsilon - 1/\varepsilon_m)$ is linearly proportional to $\ln(T - T_m)$ when ε_m and T_m are determined. The γ value can be acquired from the slope. Fig. 8 shows a graph of $\ln(1/\varepsilon - 1/\varepsilon_m)$ versus $\ln(T - T_m)$. It is obvious that the 0.93KNN–0.07LTN–*x*NN ceramics show a linear relationship between $\ln(1/\varepsilon - 1/\varepsilon_m)$ and $\ln(T - T_m)$. The γ values were therefore calculated by the least-squares fitting method. As the NN content increases, γ increases from 1.2 at $x = 0.01$ to 1.9 at $x = 0.07$. This result means that the relaxor characteristic is enhanced by increasing the NN content. The relaxor behavior can be induced in many ways, such as microscopic composition fluctuation, the merging of micro-domains into macro-domains, or a coupling of the order parameter and local disorder mode through the local strain. Na, K, and Li ions occupy the A sites of the ABO_3-typed perovskite structure, while Ta and Nb ions occupy the B sites. Therefore, the cation disorder in the perovskite unit cell should be one of the reasons for the appearance of relaxor states. Furthermore, as mentioned in Fig. 5, there are some irregular large grains grown from plate-like NN in the ceramics. The greater the content of NN, the higher is the proportion of large grains. So the strengthened relaxor behavior can be attributed to the microscopic composition fluctuation intensified by these large grains.

The Curie temperature T_C and piezoelectric properties as a function of the NN content are shown in Figs. 9 and 10. It can be seen that the Curie temperature T_C decreases from 440 °C to 408 °C with increasing amounts of NN. The electromechanical coupling factor (k_p) and the piezoelectric constant (d_{33}) show small variations as the content of NN is reduced below 0.03 mol. When the NN content is higher than 0.03 mol, k_p and d_{33} decrease rapidly. It is observed

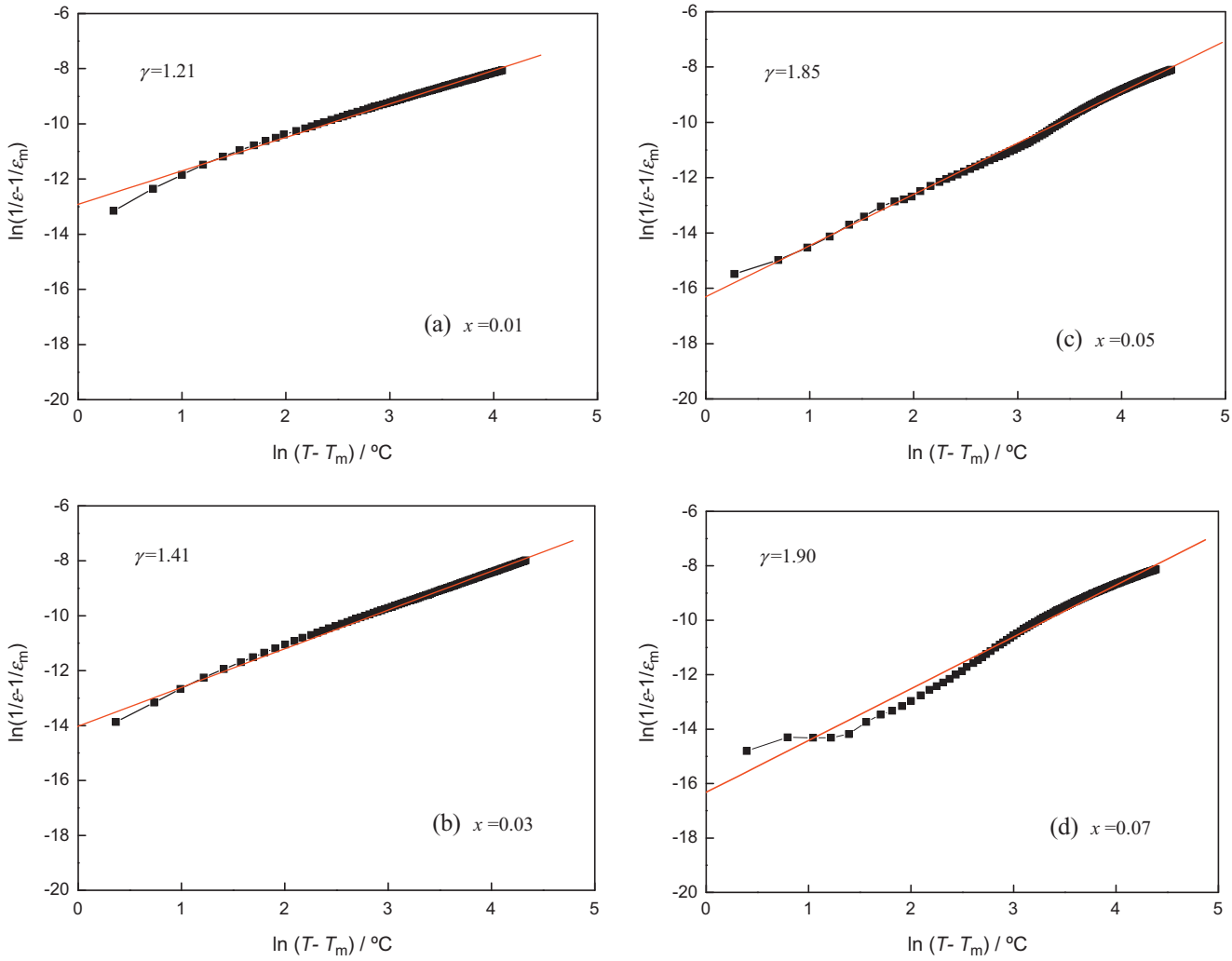

Fig. 8. $\ln(1/\varepsilon - 1/\varepsilon_m)$ as a function of $\ln(T - T_m)$ at 10 kHz for 0.93KNN–0.07LTN–*x*NN ceramics.

that the mechanical quality factor Q_m varies in the range 40–60 as *x* changes from 0.01 to 0.07. This indicates that adding too much NN will result in a composition fluctuation far from the morphotropic phase boundary, tending to weaken piezoelectric properties of the matrix material. Additionally, for the KNN-based ceramics, the phase transitions depend not only on the compositions, but also on the temperature. The polymorphic phase transition at room temperature also plays an important role in KNN-based materials [30]. The 0.93KNN–0.07LTN–*x*NN ceramics with increasing *x* shift the orthorhombic and tetragonal polymorphic phases to far away from

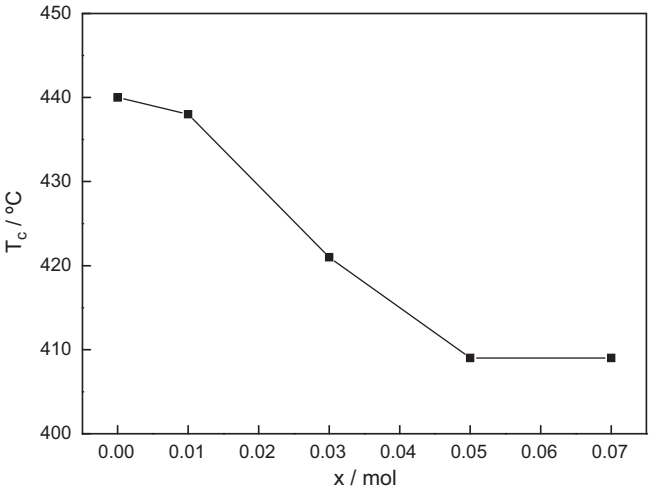

Fig. 9. Curie temperature as a function of NN content for 0.93KNN–0.07LTN–*x*NN ceramics.

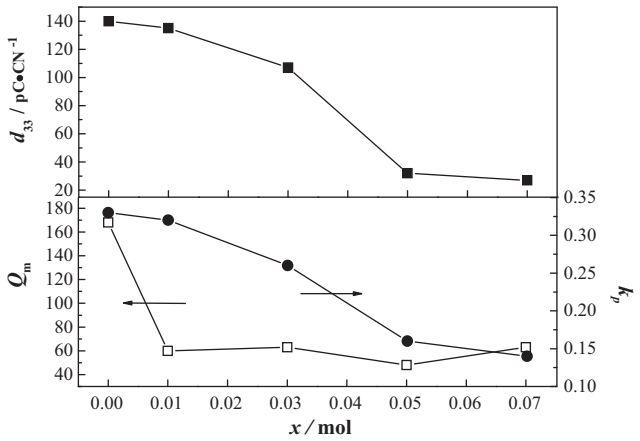

Fig. 10. Piezoelectric properties as a function of NN content for 93KNN–7LTN–*x*NN ceramics.

that of room temperature, as shown in Fig. 7. Therefore, it deteriorates piezoelectric properties at room temperature with increasing content of NN. What is more, the second phase of the tungsten bronze type $K_3Li_2Nb_5O_{15}$, with poor dielectric properties, is also responsible for the deteriorating piezoelectric properties.

The results therefore suggest that the proportion of plate-like $NaNbO_3$ in the 0.93KNN–0.07LTN ceramics cannot be increased beyond 0.03 mol. Values of 0.01–0.03 mol of the plate-like $NaNbO_3$ should be the appropriate amounts to use as templates for the RTGG method of texturing $0.93\,K_{0.48}Na_{0.52}NbO_3$–$0.07Li(Ta_{0.5}Nb_{0.5})O_3$ ceramics.

4. Conclusions

$(1-x)[0.93\,K_{0.48}Na_{0.52}NbO_3$–$0.07Li(Ta_{0.5}Nb_{0.5})O_3]$–$xNaNbO_3$ lead-free piezoelectric ceramics were fabricated by a conventional ceramic process using plate-like $NaNbO_3$ (NN) particles. The perovskite phase and $K_3Li_2Nb_5O_{15}$ phase with tungsten bronze structure coexist in the ceramics. The substitution of $NaNbO_3$ makes the crystalline symmetry of the 0.93KNN–0.07LTN–xNN perovskite structure change from coexisting tetragonal and orthorhombic perovskite phases to pseudocubic phase. The dielectric constant (ε) decreases and then increases with increasing NN content, while the dielectric loss ($\tan\delta$) continuously increases. The Curie temperature (T_C) shifts to lower temperature. Diffuse phase transition and frequency dispersion were clearly seen for the 0.93KNN–0.07LTN–xNN ceramics with $x > 0.03$, and the relaxor behavior of the ceramics is strengthened by increasing the NN content. Both the electromechanical coupling factor (k_p) and the piezoelectric constant (d_{33}) decrease with increasing amounts of NN. 0.01–0.03 mol of plate-like $NaNbO_3$ is the optimum content to prepare $0.93\,K_{0.48}Na_{0.52}NbO_3$–$0.07Li(Ta_{0.5}Nb_{0.5})O_3$ textured ceramics by the RTGG method.

Acknowledgements

This work was supported by Aviation Science Foundation of China, and Basic Research Foundation of Northwestern Polytechnical University.

References

[1] E. Cross, Nature 432 (2004) 24–25.
[2] F. Azough, M. Wegrzyn, R. Freer, S. Sharma, D. Hall, J. Eur. Ceram. Soc. 31 (2011) 569–576.
[3] Q. Zhang, B.P. Zhang, H.T. Li, P.P. Shang, J. Alloys Compd. 490 (2010) 260–263.
[4] K.C. Singh, C. Jiten, R. Laishram, O.P. Thakur, D.K. Bhattacharya, J. Alloys Compd. 496 (2010) 717–722.
[5] R. López, F. González, M.E. Villafuerte-Castrejón, J. Eur. Ceram. Soc. 30 (2010) 1549–1553.
[6] N. Jiang, B. Fang, J. Wu, Q.B. Du, J. Alloys Compd. 509 (2011) 2420–2424.
[7] H.Q. Wang, R.Z. Zuo, J. Fu, Y. Liu, J. Alloys Compd. 509 (2011) 936–994.
[8] Y. Wang, Q. Liu, F. Zhao, J. Alloys Compd. 489 (2010) 175–178.
[9] X.H. Li, J.L. Zhu, M.S. Wang, Y.S. Luo, W. Shi, L.H. Li, J.G. Zhu, D.Q. Xiao, J. Alloys Compd. 499 (2010) L1–L4.
[10] K. Kakimoto, K. Ando, H. Ohsato, J. Eur. Ceram. Soc. 30 (2010) 295–299.
[11] X.P. Jiang, Q. Yang, Z.D. Yu, F. Hua, C. Chen, N. Tu, Y.M. Li, J. Alloys Compd. 493 (2010) 276–280.
[12] Y. Saito, H. Takao, T. Tani, T. Nonoyama, K. Takatori, T. Homma, T. Nagaya, M. Nakamura, Nature 432 (2004) 84–87.
[13] H.X. Yan, H.T. Zhang, R. Ubic, M.J. Reece, J. Liu, Z.J. Shen, Z. Zhang, Adv. Mater. 17 (2005) 1261–1265.
[14] K. Fuse, T. Kimura, J. Am. Ceram. Soc. 89 (2006) 1957–1964.
[15] F. Gao, R.Z. Hong, J. Liu, Y.H. Yao, C.S. Tian, J. Eur. Ceram. Soc. 28 (2008) 2063–2070.
[16] T. Sato, Y. Yoshida, T. Kimura, J. Am. Ceram. Soc. 90 (2007) 3005–3008.
[17] S.H. Hong, S. Trolier-McKinstry, G.L. Messing, J. Am. Ceram. Soc. 83 (2000) 113–118.
[18] T. Shoji, K. Fuse, T. Kimura, J. Am. Ceram. Soc. 92 (2009) S140–S145.
[19] Z.Q. Deng, F. Gao, L.L. Liu, L. Yang, C.S. Tian, Piezoelectr. Acoustoopt. 32 (2010) 1021–1023.
[20] Y.F. Chang, Z.P. Yang, X.L. Chao, Z.H. Liu, Z.L. Wang, Mater. Chem. Phys. 111 (2008) 195–200.
[21] F. Gao, R.Z. Hong, J. Liu, Y.H. Yao, C.S. Tian, J. Electroceram. 24 (2010) 145–152.
[22] J.G. Wu, T. Peng, Y.Y. Wang, D.Q. Xiao, J.M. Zhu, Y. Jin, J.G. Zhu, P. Yu, L. Wu, Y.H. Jiang, J. Am. Ceram. Soc. 91 (2008) 319–321.
[23] F. Rubio-Marcos, P. Marchet, T. Merle-Méjean, J.F. Fernandez, Mater. Chem. Phys. 123 (2010) 91–97.
[24] F. Rubio-Marcos, M.G. Navarro-Rojero, J.J. Romero, P. Marchet, J.F. Fernández, IEEE Trans. Ultrason. Ferroelectr. Freq. 56 (2009) 1835–1842.
[25] D.J. Gao, K.W. Kwok, D.M. Lin, H.L.W. Chan, J. Mater. Sci. 44 (2009) 2466–2470.
[26] R.E. Eitel, C.A. Randall, T.R. Shrout, P.W. Rehrig, W. Hackenberger, S.E. Park, Jpn. J. Appl. Phys. 40 (2001) 5999–6002.
[27] J.G. Wu, D.Q. Xiao, Y.Y. Wang, J.G. Zhu, W. Shi, W.J. Wu, B. Zhang, J. Li, J. Alloys Compd. 476 (2009) 782–786.
[28] D.M. Lin, K.W. Kwok, H.L.W. Chan, Appl. Phys. A 91 (2008) 167–171.
[29] J. Hao, Z. Xu, R. Chu, W. Li, G.R. Li, Q.R. Yin, J. Alloys Compd. 484 (2009) 233–238.
[30] J.G. Wu, Y.Y. Wang, D.Q. Xiao, J.G. Zhu, Z.H. Pu, Appl. Phys. Lett. 91 (2007), 132914-1-3.